ISA Transactions xxx (xxxx) xxx

Contents lists available at ScienceDirect

ISA Transactions

journal homepage: www.elsevier.com/locate/isatrans

Research article

Design of shifting state-feedback controllers for LPV systems subject to time-varying saturations via parameter-dependent Lyapunov functions

Adrián Ruiz [a,*], Damiano Rotondo [b], Bernardo Morcego [a]

[a] Research Center for Supervision, Safety and Automatic Control, Universitat Politècnica de Catalunya (UPC), Rambla Sant Nebridi, 22, 08222 Terrassa, Spain

[b] Department of Electrical and Computer Engineering (IDE), University of Stavanger (UiS), Kristine Bonnevies vei 22, 4021 Stavanger, Norway

ARTICLE INFO

Article history:
Received 16 December 2020
Received in revised form 14 July 2021
Accepted 15 July 2021
Available online xxxx

Keywords:
Linear parameter varying (LPV) systems
Linear matrix inequalities (LMIs)
Shifting paradigm
Actuator saturation
Invariant ellipsoids

ABSTRACT

This paper considers the problem of designing a shifting state-feedback controller via quadratic parameter-dependent Lyapunov functions (QPDLFs) for systems subject to symmetric time-varying saturations. By means of the linear parameter varying (LPV) framework and the use of the shifting paradigm and the ellipsoidal invariant theory, it is shown that the solution to this problem can be expressed with linear matrix inequalities (LMIs) which can efficiently be solved via available solvers. Specifically, three hyper-ellipsoidal regions are defined in the state-space domain for ensuring that the control action remains in the linearity region of the actuators where saturation does not occur. Furthermore, the closed-loop convergence speed is regulated online according to the instantaneous saturation limit values through the shifting paradigm concept. The main characteristics of the proposed approach are validated by means of two illustrative examples.

1. Introduction

All real-world systems' performances are affected negatively by the inherent physical limitations of actuators. Among these limitations, actuator saturations arise in control systems as progressively decreasing actuation signals due to, for example, temporary shortages in the availability of the required power. If saturations are not taken into account properly, they may cause actuator performance deterioration and even lead to the instability of the closed-loop system. For this reason, in the last decades this phenomenon has attracted a strong attention by several researchers, which is supported by the large amount of books about this topic, see [1–3]. Actuator saturations can be taken into account through the *anti-windup compensator* approach, in which a pre-designed controller can handle the saturation constraints after a compensator is added [4,5]. On the other hand, alternative solutions use the *direct control design* approach where the input saturation constraints are considered directly in the controller design stages [6,7].

In recent years, the linear parameter varying (LPV) framework has been applied widely to address the presence of nonlinearities in various fields such as automotive, robotics, or aerospace, see [8] and references therein. These systems were introduced by *Shamma* in 1988 as a particular case of linear time varying (LTV) systems where the time-varying elements are dependent upon quantifiable parameters which vary over time [9,10]. Nonlinear systems can be represented within this framework through an appropriate definition of the time-varying parameters, which let us embed the nonlinearities through parameters that are dependent on endogenous signals. In this situation, the system is referred to as quasi-LPV, in order to emphasize the fact that the varying parameters are not dependent on exogenous signals. Three different ways to model these systems have emerged as the most successful ones in the literature, i.e. linear fractional transformation (LFT), LPV input–output models and the polytopic approach. Furthermore, the LPV framework has been applied successfully in many plants where, e.g., the parametrization of the nonlinearities allows the controller to take into account the generator shaft speed and wind speed variations improving the conversion efficiency in variable-speed wind energy conversion systems [11] or the suspension's deflections in a semi-active suspension control of a vehicle [12].

Note that the existing works assume commonly that the actuator saturation limits are constant in time. For instance, a health-aware control based on the remaining useful life estimation of a battery has been designed for an autonomous racing vehicle assuming that the input/output limits are constant [13]. The same assumption holds for [14], where a model predictive

* Corresponding author.
E-mail addresses: adrian.ruiz.royo@upc.edu (A. Ruiz), damiano.rotondo@uis.no (D. Rotondo), bernardo.morcego@upc.edu (B. Morcego).

https://doi.org/10.1016/j.isatra.2021.07.025

Please cite this article as: A. Ruiz, D. Rotondo and B. Morcego, Design of shifting state-feedback controllers for LPV systems subject to time-varying saturations via parameter-dependent Lyapunov functions. ISA Transactions (2021), https://doi.org/10.1016/j.isatra.2021.07.025.

control (MPC) algorithm has been developed for polytopic LPV systems subject to input saturations. On the other hand, some works have proposed to use a saturation indicator parameter to schedule the input constraints whose limits are still constant in time [15,16]. The lack of literature addressing time-varying saturations motivates us to consider the possible degradation of the actuators over time, which would affect the online performance of the designed controller. It is worth highlighting that, practically speaking, time-varying saturation limits could occur in control systems due to the natural wear and tear of the machinery or to the temporary loss of energy availability. This fact would provide a progressively decreasing availability of the actuation signal in the case of multi-rotor vehicles, such as the loss of thrust force in each rotor due to the discharge of the battery [17] or the variations of the aerodynamic coefficients as a consequence of environment changes [18].

With the goal of designing a state-feedback controller with the ability to regulate the closed-loop convergence speed online according to the instantaneous saturation limits, a linear matrix inequality (LMI)-based methodology has been proposed in [19]. Similarly, a shifting $\mathcal{H}_\infty$ LPV state-feedback controller has been developed in [20], where the designed controller could adapt its disturbance rejection performance online taking into account the control action availability. In both works, the overall design has been performed using a quadratic Lyapunov function (QLF) and the *ellipsoidal invariant* theory [21]. Furthermore, these works have exploited the *shifting paradigm* concept which was introduced in [22] for polytopic LPV systems, thus defining a scheduling parameter vector that allows changing online the closed-loop performance index under consideration. Nevertheless, it is well known that the use of QLFs introduces some conservativeness that can lead to sub-optimal performance or even make the design problem infeasible. This issue can be alleviated by considering parameter-dependent Lyapunov functions (PDLFs) [23–26], piecewise functions [27] or polyhedral functions [28], although at the cost of increasing the computational burden.

The main contribution of this work lies in proposing an LMI-based methodology for designing a shifting state-feedback controller via a quadratic parameter-dependent Lyapunov function (QPDLF), thus overcoming the conservativeness of the design methodology presented in [19]. The design conditions are obtained through the application of the *invariant ellipsoidal* theory and the *shifting paradigm* concept. In particular, three hyper-ellipsoidal regions are defined in the state-space domain for ensuring that the control action remains in the linearity region of the actuators. Furthermore, the shifting paradigm is used to schedule the convergence speed of the closed-loop system response according to the instantaneous saturation limit values. The LMI conditions are obtained by applying Schur complements [21] together with the Pólya's relaxation inherited from [29]. The final solution is a set of LMIs that can be solved using available solvers, and which are less conservative than the set provided in [19], as demonstrated by the examples, showcasing both a comparison using a numerical example and a proof of concept with a nonlinear quadrotor model.

The paper is organized as follows. The problem formulation is provided in Section 2. In Section 3, the LMI-based methodology for the controller design is given. In Section 4, the design implementation procedure is summarized. In Section 5, simulation results are presented using a numerical system and the nonlinear quadrotor model. Finally, the main conclusions and perspectives on future research are outlined in Section 6.

1.1. Notation

For a real symmetric matrix $M \in \mathbb{R}^{m\times m}$, the notation $M \succ 0$ ($M \succeq 0$) stands for a positive (semi-)definite matrix and indicates that all the eigenvalues of M are positive (non-negative). In the same way, $M \prec 0$ ($M \preceq 0$) denotes a negative (semi-)definite matrix, which implies that all the eigenvalues of M are negative (non-positive). The symbols I_n, $diag(\dots)$ and $\otimes$ denote the n-dimensional identity matrix, a diagonal matrix and the Kronecker product of matrices [30], respectively. Moreover, $He\{A\} = A + A^T$ where A^T is the transpose of A. Finally, given the Pólya's relaxation degree $d \in \mathbb{N}$ with $d \geq 2$ and the number of vertices N, the symbols $\mathbb{P}_{(d,N)}$ and $\mathbb{P}^+_{(d,N)}$ denote the following sets:

$$\mathbb{P}_{(d,N)} \triangleq \left\{\vec{q} = [q_1, \dots, q_d] \in \mathbb{N}^d \mid 1 \leq q_k \leq N \ \forall k = 1, \dots, d\right\}, \tag{1}$$

$$\mathbb{P}^+_{(d,N)} \triangleq \left\{\vec{q} \in \mathbb{P}_{(d,N)} \mid q_k \leq q_{k+1}\ k = 1, \dots, d-1\right\}, \tag{2}$$

whereas $\mathcal{P}(\vec{q}) \subset \mathbb{P}_{(d,N)}$ corresponds to the set of permutations, with possible repeated elements, of multi-index $\vec{q}$.

2. Problem statement

Let us look at the following continuous-time saturated LPV system:

$$\dot{x}(t) = A(\vartheta(t))x(t) + B(\vartheta(t))sat(u(t), \sigma(t)), \tag{3}$$

where $x(t) \in \mathbb{R}^{n_x}$ is the state vector and $u(t) \in \mathbb{R}^{n_u}$ denotes the control input vector. $A(\vartheta(t)) \in \mathbb{R}^{n_x\times n_x}$ and $B(\vartheta(t)) \in \mathbb{R}^{n_x\times n_u}$ denote the state and the input matrices, respectively, which depend on a scheduling parameter vector $\vartheta(t) \in \Theta \subset \mathbb{R}^{n_\vartheta}$, with set Θ known, closed and bounded. Moreover, $\vartheta(t)$ is assumed throughout this work to be continuously differentiable for $t \geq 0$ in order to guarantee the existence of $\dot{\vartheta}(t)$, and it is assumed that $\dot{\vartheta}(t) \in \Theta_d \subset \mathbb{R}^{n_\vartheta}$, with set Θ_d known, closed and bounded.

The input $u(t)$ in (3) is affected by symmetric input saturations with time-varying limits:

$$sat(u_h(t), \sigma_h(t)) = sign(u_h(t))\min(|u_h(t)|, \sigma_h(t)), \tag{4}$$

where $h = 1, \dots, n_u$ and $\sigma_h(t) \in \mathbb{R}^{n_u}_+$ is the instantaneous saturation limit value. $\sigma_h(t)$ takes values within the interval $[\underline{\sigma}_h,\ \overline{\sigma}_h]$, where $\underline{\sigma}_h$ is the lowest possible saturation limit and $\overline{\sigma}_h$ is the highest possible saturation limit for each input $u_h(t)$. Hence, the linear region of the actuators $\mathcal{L}(t) \subset \mathbb{R}^{n_u}$, defined as the hypercube region of the input space in which $u(t)$ does not saturate, is time-varying and given by:

$$\mathcal{L}(t) \triangleq \{-\sigma_1(t),\ \sigma_1(t)\} \times \dots \times \{-\sigma_h(t),\ \sigma_h(t)\}, \tag{5}$$

where $\times$ denotes the Cartesian product and $\{-\sigma_h(t),\ \sigma_h(t)\}$ indicates the corresponding set of each instantaneous saturation limit value $\forall h = 1, \dots, n_u$.

Before stating the problem formally (Section 2.5), let us introduce the polytopic representation, the shifting paradigm, the performance criterion and the established region constraints.

2.1. Polytopic representation

In the rest of the work, a polytopic representation of the system (3) will be used, according to the following definition.

Definition 1 (*Apkarian and Gahinet [31]*)**.** The LPV system (3) is said to be *polytopic* if it can be represented by state-space matrices whose dependence on the scheduling parameter vector $\vartheta(t)$ satisfies:

$$\begin{bmatrix} A(\vartheta(t)) & B(\vartheta(t)) \end{bmatrix} \in Co\left\{\begin{bmatrix} A_i & B_i \end{bmatrix}\right\},\ \forall i = 1, \dots, N, \tag{6}$$

with $Co\{[A_i \quad B_i]\}$ representing the convex hull of a finite number of N vertex matrices:

$$\left\{\sum_{i=1}^{N}\mu_i(\vartheta(t))\begin{bmatrix}A_i & B_i\end{bmatrix} : \sum_{i=1}^{N}\mu_i(\vartheta(t)) = 1,\ \mu_i(\vartheta(t)) \geq 0,\ \forall i = 1,\ldots,N\right\}. \tag{7}$$

Note that, taking into account the knowledge of the bounds of Θ and Θ_d, $\dot{\mu}_i(\vartheta(t))\ \forall i = 1,\ldots,N$ can be bounded as follows:

$$\underline{v}_i \leq \dot{\mu}_i(\vartheta(t)) \leq \overline{v}_i, \tag{8}$$

with known bounds $\underline{v}_i, \overline{v}_i \in \mathbb{R}$.

2.2. Shifting paradigm

The shifting paradigm was presented in [22] as a possible approach to take advantage of the properties of polytopes and LMIs, enabling the design of a gain-scheduling controller that adapts the performance of the closed-loop system online depending on some chosen criteria, e.g., guaranteed decay rate, pole clustering or $\mathcal{H}_\infty/\mathcal{H}_2$ bounds. This paradigm has been used recently in [19] and [20] for describing the time-varying saturation in polytopic form by introducing a new scheduling parameter vector $\varphi(t) \in \Phi \subset \mathbb{R}^{n_\varphi}$. Roughly speaking, $\varphi(t)$ was used to increase/decrease online the convergence speed [19] or the disturbance effectiveness [20] of the closed-loop system according to the instantaneous value of $\sigma_h(t)$. In this way, a faster response or a better disturbance rejection can be guaranteed when a large control action is available ($\sigma_h(t) \to \overline{\sigma}_h$) whereas the controller will provide a more conservative performance when the instantaneous value of $\sigma_h(t)$ is closer to $\underline{\sigma}_h$. Then, the time-varying limit changes in (4) can be described by the scheduling parameter $\varphi(t)$, which is chosen to be a weighted function of $\sigma_h(t)$, for example taking values within the interval [0, 1].

Similarly to the case of $\vartheta(t)$, the matrices which depend on $\varphi(t)$ and satisfy $T(\varphi(t)) \in Co\{T_j\}$ can be described as follows:

$$Co\{T_j\} \triangleq \left\{\sum_{j=1}^{M}\eta_j(\varphi(t))T_j : \sum_{j=1}^{M}\eta_j(\varphi(t)) = 1,\ \eta_j(\varphi(t)) \geq 0,\ \forall j = 1,\ldots,M\right\}, \tag{9}$$

where M is the number of vertices of the polytope Φ and, $T(\varphi(t))$ and T_j correspond to the chosen polytope and vertex matrices, respectively.

Additionally, the time-derivative of this new scheduling parameter vector is assumed to satisfy $\dot{\varphi}(t) \in \Phi_d \subset \mathbb{R}^{n_\varphi}$, with set Φ_d known, closed and bounded, so that the following holds $\forall j = 1,\ldots,M$:

$$\underline{p}_j \leq \dot{\eta}_j(\varphi(t)) \leq \overline{p}_j, \tag{10}$$

with known bounds $\underline{p}_j,\ \overline{p}_j \in \mathbb{R}$.

2.3. Performance criterion

Let us consider the following LPV state-feedback control law for (3) and the quadratic parameter-dependent Lyapunov function (QPDLF) which depends on the scheduling parameter vectors $\vartheta(t)$ and $\varphi(t)$:

$$u(t) = K(\vartheta(t),\varphi(t))x(t), \tag{11}$$

$$V(x(t),\vartheta(t),\varphi(t)) = x(t)^T P(\vartheta(t),\varphi(t))x(t), \tag{12}$$

where $K(\vartheta(t),\varphi(t)) \in \mathbb{R}^{n_u\times n_x}$ is the parameter-dependent controller gain and $P(\vartheta(t),\varphi(t)) \in \mathbb{R}^{n_x\times n_x}$ denotes a positive definite parameter-dependent Lyapunov matrix.

Then, based on the shifting paradigm idea and the above defined QPDLF (12), let us define the performance criterion considered throughout this work.[1]

Definition 2 (*Guaranteed Shifting Decay Rate*)**.** The LPV system (3) with state-feedback control law (11) is said to satisfy the *guaranteed shifting decay rate* $\lambda(\vartheta,\varphi)$ with the parameter-dependent matrix $P(\vartheta,\varphi)$, if:

$$\dot{V}(x,\vartheta,\varphi) \leq -2\lambda(\vartheta,\varphi)V(x,\vartheta,\varphi). \tag{13}$$

By means of the above defined performance criterion the shifting state-feedback controller (11) ensures the closed-loop exponential stability of the LPV system (3) if $\lambda(\vartheta,\varphi) \in \mathbb{R}_+$. Moreover, the closed-loop response of (3) adapts its behaviour online, in the sense that the convergence speed will change online according to the instantaneous value taken by $\lambda(\vartheta,\varphi)$. However, the fulfilment of the Lyapunov condition (13) is conditioned to the use of a nonlinear expression of $u(t)$ complicating the obtention of computationally applicable design conditions. This issue can be alleviated by ensuring that $u(t) \in \mathcal{L}(t)\ \forall t \geq 0$, thus allowing to neglect the saturation nonlinearity during the design stage.

2.4. Region constraints

The approach used to guarantee that $u(t) \in \mathcal{L}(t)$ is based on the definition of appropriate hyper-ellipsoidal regions. Consider the parameter-varying set $\mathcal{U}(\varphi) \subset \mathbb{R}^{n_u}$ defined as the maximal hyper-ellipsoidal region contained in $\mathcal{L}(t)$, as follows:

$$\mathcal{U}(\varphi) \triangleq \left\{u \in \mathbb{R}^{n_u} : u^T S(\varphi)u \leq 1\right\}, \tag{14}$$

where $S(\varphi) \in \mathbb{R}^{n_u\times n_u}$ is a known matrix function that defines the parameter-varying orientation and size of the region $\mathcal{U}(\varphi)$. Due to the LPV state-feedback control law (11), the region $\mathcal{U}(\varphi)$ can be mapped to a corresponding state-space region $\mathcal{U}_x(\vartheta,\varphi)$, as follows:

$$\mathcal{U}_x(\vartheta,\varphi) \triangleq \left\{x \in \mathbb{R}^{n_x} : x^T K(\vartheta,\varphi)^T S(\varphi)K(\vartheta,\varphi)x \leq 1\right\}. \tag{15}$$

Let us define $\mathcal{V}(\vartheta,\varphi)$ as the parameter-dependent region of the state-space that is delimited by the unit level curves of the QPDLF (12) and $\mathcal{E}$ as the region of the state-space which contains the initial conditions of interest for the system:

$$\mathcal{V}(\vartheta,\varphi) \triangleq \left\{x \in \mathbb{R}^{n_x} : x^T P(\vartheta,\varphi)x \leq 1\right\} \tag{16}$$

$$\mathcal{E} \triangleq \left\{x \in \mathbb{R}^{n_x} : x^T X_0 x \leq 1\right\}, \tag{17}$$

where $X_0 \in \mathbb{R}^{n_x\times n_x}$ with $X_0 \succ 0$ defines the size and orientation of $\mathcal{E}$.

The hyper-ellipsoidal regions described in (15)–(17) must satisfy inclusions:

$$\mathcal{E} \subseteq \mathcal{V}(\vartheta,\varphi) \subseteq \mathcal{U}_x(\vartheta,\varphi) \tag{18}$$

in order to guarantee that $u(t)$ does not saturate $\forall t > 0$ during the transient response of $x(t)$ no matter the initial state $x(0) \in \mathcal{E}$.

[1] Hereafter, the time dependency of x, u, ϑ and φ is dropped to simplify the notation, and it will be made explicit only when needed to avoid misinterpretations.

If (18) holds, the LPV system with saturations (3) can be reduced to the following non-saturated LPV system for design purposes:

$$\dot{x}(t) = A(\vartheta(t))x(t) + B(\vartheta(t))u(t). \tag{19}$$

2.5. Problem definition

Finally, on the basis of the performance criterion (Definition 2) and the region constraints established in (18), the design problem considered in this paper can be formulated as follows:

Problem 1. Given the polytopic LPV system (3) and (6) subject to the time-varying saturations (4), a desired guaranteed shifting decay rate $\lambda(\vartheta,\varphi)$ and the regions (15)–(17), find $P(\vartheta,\varphi)$ and $K(\vartheta,\varphi)$ such that for any $x(0) \in \mathcal{E}$ the response of the closed-loop LPV system satisfies (13).

Remark 1. In this paper, in order to keep the mathematical complexity somehow limited, the presence of external disturbances is not considered. The interested reader is referred to [20], where a shifting $\mathcal{H}_\infty$ LPV state-feedback controller has been designed to ensure that a polytopic LPV system subject to symmetric time-varying input saturation is quadratically bounded with respect to unknown disturbances. The extension to the parameter-dependent case of quadratic boundedness or similar robust techniques goes beyond the scope of this paper and will be addressed in future work.

3. Shifting LPV state-feedback synthesis

Let us start by introducing the following theorem which gives a parameter-dependent LMI for designing a parameter-dependent controller gain that ensures some desired guaranteed shifting decay rate.

Theorem 1. *Consider the continuous-time LPV system (19), the control law (11) and the QPDLF in (12), and assume that there exist a positive symmetric matrix function $Q(\vartheta,\varphi) \in \mathbb{R}^{n_x \times n_x}$ and a parameter-dependent matrix $\Gamma(\vartheta,\varphi) \in \mathbb{R}^{n_u \times n_x}$ such that the following parameter-dependent LMI is satisfied:*

$$\begin{aligned} &He\{A(\vartheta)Q(\vartheta,\varphi) + B(\vartheta)\Gamma(\vartheta,\varphi)\} \\ &\quad - \dot{Q}(\vartheta,\varphi) + 2\lambda(\vartheta,\varphi)Q(\vartheta,\varphi) \preceq 0. \end{aligned} \tag{20}$$

Then, if the controller gain is computed as $K(\vartheta,\varphi) = \Gamma(\vartheta,\varphi)P(\vartheta,\varphi)$, the closed-loop LPV system satisfies the guaranteed shifting decay rate $\lambda(\vartheta,\varphi)$ with the parameter-dependent matrix $P(\vartheta,\varphi) = Q(\vartheta,\varphi)^{-1}$.

Proof of Theorem 1. By introducing the control law (11) into the system's equation (19), the following LPV closed-loop system representation is obtained:

$$\dot{x} = (A(\vartheta) + B(\vartheta)K(\vartheta,\varphi))\,x = A_{cl}(\vartheta,\varphi)x, \tag{21}$$

where $A_{cl}(\vartheta,\varphi)$ denotes the closed-loop parameter-dependent state matrix.

Then, let us calculate $\dot{V}(x,\vartheta,\varphi)$ from the expression described by (12), thus obtaining:

$$\dot{V}(x,\vartheta,\varphi) = \dot{x}^T P(\vartheta,\varphi)x + x^T P(\vartheta,\varphi)\dot{x} + x^T \dot{P}(\vartheta,\varphi)x. \tag{22}$$

By replacing (21) in (22), the following expression for $\dot{V}(x,\vartheta,\varphi)$ is obtained:

$$\begin{aligned} \dot{V}(x,\vartheta,\varphi) = x^T &\left(A_{cl}(\vartheta,\varphi)^T P(\vartheta,\varphi) + P(\vartheta,\varphi)A_{cl}(\vartheta,\varphi)\right)x \\ &+ x^T \dot{P}(\vartheta,\varphi)x. \end{aligned} \tag{23}$$

In order to ensure that the LPV closed-loop system response of (21) satisfies a guaranteed decay rate $\lambda(\vartheta,\varphi)$, $\dot{V}(x,\vartheta,\varphi)$ must satisfy the inequality (13), thus obtaining:

$$He\{P(\vartheta,\varphi)A_{cl}(\vartheta,\varphi)\} + \dot{P}(\vartheta,\varphi) + 2\lambda(\vartheta,\varphi)P(\vartheta,\varphi) \preceq 0. \tag{24}$$

Then, by pre- and post-multiplying (24) by $Q(\vartheta,\varphi)$, one gets the following inequality:

$$\begin{aligned} &He\{A_{cl}(\vartheta,\varphi)Q(\vartheta,\varphi)\} + Q(\vartheta,\varphi)\dot{P}(\vartheta,\varphi)Q(\vartheta,\varphi) \\ &\quad + 2\lambda(\vartheta,\varphi)Q(\vartheta,\varphi) \preceq 0, \end{aligned} \tag{25}$$

which is equivalent to:

$$He\{A_{cl}(\vartheta,\varphi)Q(\vartheta,\varphi)\} - \dot{Q}(\vartheta,\varphi) + 2\lambda(\vartheta,\varphi)Q(\vartheta,\varphi) \preceq 0, \tag{26}$$

where $\dot{Q}(\vartheta,\varphi) = -Q(\vartheta,\varphi)\dot{P}(\vartheta,\varphi)Q(\vartheta,\varphi)$ [32,33] has been used. Then, by replacing (21) in (26), the following is obtained:

$$\begin{aligned} &He\{A(\vartheta)Q(\vartheta,\varphi) + B(\vartheta)K(\vartheta,\varphi)Q(\vartheta,\varphi)\} - \dot{Q}(\vartheta,\varphi) \\ &\quad + 2\lambda(\vartheta,\varphi)Q(\vartheta,\varphi) \preceq 0, \end{aligned} \tag{27}$$

which is a bilinear matrix inequality (BMI) due to the product between the decision variables $K(\vartheta,\varphi)$ and $Q(\vartheta,\varphi)$. In order to transform it into a parameter-dependent LMI, the change of variable $\Gamma(\vartheta,\varphi) = K(\vartheta,\varphi)Q(\vartheta,\varphi)$ is used, thus obtaining (20). ■

Note that the parameter-dependent LMI (20) represents an infinite number of constraints, which can be converted into a finite number of LMIs by considering the polytopic assumption. To this end, a suitable polytopic representation for the terms $\lambda(\vartheta,\varphi)$, $\Gamma(\vartheta,\varphi)$, $Q(\vartheta,\varphi)$ and $\dot{Q}(\vartheta,\varphi)$ appearing in (20) is found.

For $\lambda(\vartheta,\varphi)$, $\Gamma(\vartheta,\varphi)$ and $Q(\vartheta,\varphi)$ such representations can be obtained straightforwardly by assuming that:

$$\lambda(\vartheta,\varphi) = \sum_{i=1}^{N}\mu_i(\vartheta)\sum_{j=1}^{M}\eta_j(\varphi)\lambda_{ij}, \tag{28}$$

$$\Gamma(\vartheta,\varphi) = \sum_{i=1}^{N}\mu_i(\vartheta)\sum_{j=1}^{M}\eta_j(\varphi)\Gamma_{ij}, \tag{29}$$

$$Q(\vartheta,\varphi) = \sum_{i=1}^{N}\mu_i(\vartheta)\sum_{j=1}^{M}\eta_j(\varphi)Q_{ij}, \tag{30}$$

where $\lambda_{ij} \in \mathbb{R}_+$, $\Gamma_{ij} \in \mathbb{R}^{n_u \times n_x}$ and $Q_{ij} \in \mathbb{R}^{n_x \times n_x}$ correspond to a desired decay rate value and two decision variables, respectively, for the pair (i,j).

Then, by differentiating the expression (30), we find out that $\dot{Q}(\vartheta,\varphi)$ can be expressed as:

$$\begin{aligned} \dot{Q}(\vartheta,\varphi) &= \sum_{i=1}^{N}\dot{\mu}_i(\vartheta)\sum_{j=1}^{M}\eta_j(\varphi)Q_{ij} + \sum_{i=1}^{N}\mu_i(\vartheta)\sum_{j=1}^{M}\dot{\eta}_j(\varphi)Q_{ij} \\ &= \sum_{i=1}^{N}\sum_{j=1}^{M}\dot{\mu}_i(\vartheta)\eta_j(\varphi)Q_{ij} + \sum_{i=1}^{N}\sum_{j=1}^{M}\mu_i(\vartheta)\dot{\eta}_j(\varphi)Q_{ij}, \end{aligned} \tag{31}$$

where $\dot{\mu}_i(\vartheta)$ and $\dot{\eta}_j(\varphi)$ vary within the defined bounds (8) and (10). According to [23–26], note that $\mu_i(\vartheta)$ and $\eta_j(\varphi)$ fulfil (7) and (9), respectively, implying that:

$$\frac{d}{dt}\left(\sum_{i=1}^{N}\mu_i(\vartheta)\right) = \sum_{i=1}^{N}\dot{\mu}_i(\vartheta) = 0, \tag{32}$$

$$\frac{d}{dt}\left(\sum_{j=1}^{M}\eta_j(\varphi)\right) = \sum_{j=1}^{M}\dot{\eta}_j(\varphi) = 0. \tag{33}$$

Moreover, it is possible to compute a finite number of O vectors $f^{\{k\}}$ and R vectors $g^{\{l\}}$ that satisfy:

$$\sum_{i=1}^{N} f_i^{\{k\}} = 0 \quad \forall k = 1, \ldots, O, \tag{34}$$

$$\sum_{j=1}^{M} g_j^{\{l\}} = 0 \quad \forall l = 1, \ldots, R, \tag{35}$$

where O and R are the number of vertices of the polytopes obtained as the intersections of the hyper-rectangles defined by the constraints (8) and (10) and the hyperplanes defined in (32) and (33), respectively. $f_i^{\{k\}}$ and $g_j^{\{l\}}$ denote the ith and jth component of each vector, such that (32) is fulfilled $\forall k = 1, \ldots, O$ and (33) holds $\forall l = 1, \ldots, R$. Then, the regions where $\dot{\mu}_i(\vartheta)$ and $\dot{\eta}_j(\varphi)$ lie can be described as the convex hull of $f^{\{k\}}$ and $g^{\{l\}}$ as follows:

$$\begin{bmatrix} \dot{\mu}_1(\vartheta) \\ \vdots \\ \dot{\mu}_N(\vartheta) \end{bmatrix} \in Co\left\{f^{\{k\}}\right\} \triangleq \left\{ \sum_{k=1}^{O} \alpha_k(\vartheta, \dot{\vartheta}) f^{\{k\}} : \sum_{k=1}^{O} \alpha_k(\vartheta, \dot{\vartheta}) = 1, \ \alpha_k(\vartheta, \dot{\vartheta}) \geq 0 \right\} \tag{36}$$

$$\begin{bmatrix} \dot{\eta}_1(\varphi) \\ \vdots \\ \dot{\eta}_M(\varphi) \end{bmatrix} \in Co\left\{g^{\{l\}}\right\} \triangleq \left\{ \sum_{l=1}^{R} \beta_l(\varphi, \dot{\varphi}) g^{\{l\}} : \sum_{l=1}^{R} \beta_l(\varphi, \dot{\varphi}) = 1, \ \beta_l(\varphi, \dot{\varphi}) \geq 0 \right\} \tag{37}$$

Thus, the polytopic representation of $\dot{Q}(\vartheta, \varphi)$ is:

$$\begin{aligned} \dot{Q}(\vartheta, \varphi) = & \sum_{i=1}^{N} \sum_{j=1}^{M} \sum_{k=1}^{O} \eta_j(\varphi) \alpha_k(\vartheta, \dot{\vartheta}) f_i^{\{k\}} Q_{ij} \\ & + \sum_{i=1}^{N} \sum_{j=1}^{M} \sum_{l=1}^{R} \mu_i(\vartheta) \beta_l(\varphi, \dot{\varphi}) g_j^{\{l\}} Q_{ij}, \end{aligned} \tag{38}$$

for some coefficients $\alpha_k(\vartheta, \dot{\vartheta})$ and $\beta_l(\varphi, \dot{\varphi})$ satisfying the constraints appearing in (36)–(37).

Given the above discussion, we can now introduce the following theorem which provides a finite number of LMIs that can be used to assess the parameter-dependent LMI (20).

Theorem 2. *Consider the parameter-dependent LMI (20), a finite number of vectors $f^{\{k\}}$ and $g^{\{l\}}$ for which (34)–(37) hold, and some previously chosen Pólya's relaxation degrees $d \in \mathbb{N}$ and $s \in \mathbb{N}$. If there exist matrices $Q_{i,j} \succ 0$ and $\Gamma_{i,j}$ such that the following set of LMIs is satisfied $\forall k = 1, \ldots, O$ and $\forall l = 1, \ldots, R$:*

$$\sum_{\vec{j} \in \mathcal{P}(\vec{r})} \sum_{\vec{i} \in \mathcal{P}(\vec{q})} \left[He\left\{ A_{i_1} Q_{i_2, j_1} + B_{i_2} \Gamma_{i_1, j_1} \right\} + 2\lambda_{i_1, j_1} Q_{i_2, j_2} - \Xi_{i_1, j_1} \right] \preceq 0, \tag{39}$$

where multi-indexes $\vec{q}$ and $\vec{r}$ are associated to the sets $\mathbb{P}^{+}_{(d,N)}$ and $\mathbb{P}^{+}_{(s,M)}$, respectively, and

$$\Xi_{i_1, j_1} \triangleq \sum_{m=1}^{N} f_m^{\{k\}} Q_{m, j_1} + \sum_{n=1}^{M} g_n^{\{l\}} Q_{i_1, n}, \tag{40}$$

then (20) holds with $\lambda(\vartheta, \varphi)$, $\Gamma(\vartheta, \varphi)$ and $Q(\vartheta, \varphi)$ given by (28)–(30).

Proof of Theorem 2. See Appendix A.1. ■

Remark 2. Note that the possible codependence between the coefficients $\mu_i(\vartheta)$ and $\alpha_k(\vartheta, \dot{\vartheta})$ has been neglected. The same applies to the codependence between $\eta_j(\varphi)$ and $\beta_l(\varphi, \dot{\varphi})$. Albeit introducing some conservativeness, this assumption has enabled the application of Pólya's theorem [29], so that the computational complexity during the design stage has been reduced.

Remark 3. According to [32], the fact of considering arbitrarily large values for the bounds (8) and (10) in Theorem 2 implies that the only possible solution for solving the condition (39) is to choose $Q_{11} \approx \ldots \approx Q_{NM}$, thus making the term in (40) equal to zero. In this case, the QLF $V(x) = x^T P x$ can be recovered by considering $Q \succ 0$ as the common decision variable for all the pairs (i, j) in (30).

Taking into account the theoretical results obtained so far, the following theorem provides a set of LMIs for solving Problem 1, i.e., a set of LMIs that can be used for obtaining a controller that ensures that the closed-loop response of the LPV system (3) is adapted online according to the instantaneous saturation limit values of $\sigma(t)$ through the scheduling parameter vector $\varphi(t)$. Furthermore, this theorem guarantees that the control action $u(t)$ will remain inside the linearity region of the actuators $\mathcal{L}(t)$ due to the inclusion chain described in (18). Note that the inclusion $\mathcal{E} \subseteq \mathcal{V}(\vartheta, \varphi)$ for $x(0) \in \mathcal{E}$ ensures that $x(t) \in \mathcal{V}(\vartheta, \varphi)$ $\forall t$ as long as the system works in the linear region described by (4). Also, taking into account $\mathcal{V}(\vartheta, \varphi) \subseteq \mathcal{U}_x(\vartheta, \varphi)$ any state trajectory $x(t)$ contained in $\mathcal{V}(\vartheta, \varphi)$ will also be located in $\mathcal{U}_x(\vartheta, \varphi)$, so no saturation happens and, therefore, the convergence of $x(t) \to 0$ when $t \to \infty$ is guaranteed for any $x(0) \in \mathcal{V}(\vartheta, \varphi)$, and hence for any $x(0) \in \mathcal{E}$.

Theorem 3. *Consider the continuous-time LPV system (19), the control law (11), the QPDLF in (12), the hyper-ellipsoidal regions (15)–(17) with the given matrices X_0 and $S(\varphi)$, a guaranteed decay rate $\lambda(\vartheta, \varphi)$ and finite number of vectors $f^{\{k\}}$ and $g^{\{l\}}$ for which (34)–(37) hold. Consider also that the Pólya's relaxation degree $d \in \mathbb{N}$ and $s \in \mathbb{N}$ have been selected. Furthermore, suppose that the inverse of the parameter-dependent matrix function $S(\varphi)$ can be expressed as:*

$$S(\varphi)^{-1} = \sum_{j=1}^{M} \eta_j(\varphi) S_j^{-1}, \tag{41}$$

where M denotes the number of vertices of the polytope Φ. If there exist $Q_{ij} \succ 0$ and Γ_{ij} such that the set of LMIs defined in (39) and the next set of LMIs are feasible $\forall i = 1, \ldots, N$ and $\forall j = 1, \ldots, M$

$$\begin{bmatrix} Q_{ij} & I_n \\ I_n^T & \mathcal{X}_0 \end{bmatrix} \succeq 0, \tag{42}$$

$$\begin{bmatrix} S_j^{-1} & \Gamma_{ij} \\ \Gamma_{ij}^T & Q_{ij} \end{bmatrix} \succeq 0, \tag{43}$$

then the closed-loop system response, obtained as the interconnection of (19) and (11), with controller gain calculated as $K(\vartheta, \varphi) = \Gamma(\vartheta, \varphi) Q(\vartheta, \varphi)^{-1}$ with $\Gamma(\vartheta, \varphi)$, $Q(\vartheta, \varphi)$ obtained from Γ_{ij} and Q_{ij} using (29)–(30), has a guaranteed shifting decay rate $\lambda(\vartheta, \varphi)$ given by (28) for every $x(0) \in \mathcal{E}$.

Proof of Theorem 3. The fact that (39) ensures that the closed-loop system (19) satisfies the guaranteed decay rate $\lambda(\vartheta, \varphi)$ as

long as it works in the region of linearity of the actuators, $\mathcal{L}(t)$, has been shown in the proof of Theorem 2. Hence, let us demonstrate that if the LMIs (42)–(43) hold, then $u(t)$ remains inside the region $\mathcal{U}(\varphi)$ for all t, as long as $x(0) \in \mathcal{E}$.

To this end, let us consider the inclusions in (18). The inclusion $\mathcal{E} \subseteq \mathcal{V}(\vartheta, \varphi)$ may be formulated as:

$$x^T P(\vartheta, \varphi) x \leq x^T \mathcal{X}_0 x, \tag{44}$$

which is equivalent to:

$$\mathcal{X}_0 - {I_n}^T P(\vartheta, \varphi) I_n \succeq 0 \tag{45}$$

and that, by applying Schur complements, becomes:

$$\begin{bmatrix} Q(\vartheta, \varphi) & I_n \\ {I_n}^T & \mathcal{X}_0 \end{bmatrix} \succeq 0. \tag{46}$$

Thereupon, as the parameter-dependent matrix $Q(\vartheta, \varphi)$ is described by means of (30), the set of LMIs (42) is obtained.

In the same way, taking into account (15), the inclusion $\mathcal{V}(\vartheta, \varphi) \subseteq \mathcal{U}_x(\vartheta, \varphi)$ can be rewritten as:

$$x^T K(\vartheta, \varphi)^T S(\varphi) K(\vartheta, \varphi) x \leq x^T P(\vartheta, \varphi) x. \tag{47}$$

Then, manipulating the above expression one gets:

$$P(\vartheta, \varphi) - K(\vartheta, \varphi)^T S(\varphi) K(\vartheta, \varphi) \succeq 0. \tag{48}$$

Now, let us pre- and post-multiply (48) by $Q(\vartheta, \varphi)$, thus obtaining:

$$Q(\vartheta, \varphi) - Q(\vartheta, \varphi) K(\vartheta, \varphi)^T S(\varphi) K(\vartheta, \varphi) Q(\vartheta, \varphi) \succeq 0. \tag{49}$$

By applying the change of variable $\Gamma(\vartheta, \varphi) = K(\vartheta, \varphi) Q(\vartheta, \varphi)$, and using Schur complements, (49) becomes:

$$\begin{bmatrix} S(\varphi)^{-1} & \Gamma(\vartheta, \varphi) \\ \Gamma(\vartheta, \varphi)^T & Q(\vartheta, \varphi) \end{bmatrix} \succeq 0. \tag{50}$$

Finally, the set of LMIs (43) is obtained by taking into account (29), (30) and (41), thus concluding the proof. ■

4. Design implementation procedure

Problem 1 is solved using the methodology given by Theorem 3, which corresponds to an LMI-based feasibility problem subject to the performance criterion (13), the region constraints (15)–(17) and the inclusion chain (18). The design and implementation procedure can be summarized as follows:

Off-line computation:

1. Obtain an LPV representation of the system as in (6)–(8);
2. Define the region (14) through the matrix $S(\varphi)$ taking into account the bounds of the instantaneous saturation limit values (4)–(5);
3. Express the matrix $S(\varphi)^{-1}$ as in (41);
4. Define the region (17) through the matrix X_0;
5. Choose the desired decay rate values in (28) for each pair of (i, j);
6. Obtain a finite number of vectors (34)–(35) as in (51);
7. Choose the Pólya's relaxation degrees d and s;
8. Obtain the vertex matrix values of $\Gamma(\vartheta, \varphi)$ and $Q(\vartheta, \varphi)$ by solving Theorem 3 (see Remark 4).

Online computation:

1. Compute the current polytopic weights $\mu_i(\vartheta)$ and $\eta_j(\varphi)$ for all $i = 1, \ldots, N$ and $j = 1, \ldots, M$;
2. Compute the current value of $\Gamma(\vartheta, \varphi)$ using (29);
3. Compute the current value of $Q(\vartheta, \varphi)$ using (30);
4. Compute $K(\vartheta, \varphi) = \Gamma(\vartheta, \varphi) Q(\vartheta, \varphi)^{-1}$.

Remark 4. Previous knowledge of the plant is required to define regions $\mathcal{E}$ and $\mathcal{U}(\varphi)$ described in (14) and (17) through the matrices X_0 and $S(\varphi)$, so that they have a physical meaning. These regions define the initial conditions of interest and the control action space, respectively. As a consequence of this fact, the solution of Theorem 3 is conditioned by trade-offs related to these regions, for example, a choice of the expected initial conditions closer to the origin facilitates the feasibility of the LMI-based problem, although it is desirable that the controller operates over a region of possible initial conditions as big as possible. However, from a practical point of view, this is constrained by the available range of the control action. For instance, when a wide range of control action is available, a larger region of initial conditions could be considered while maintaining feasibility of the solution.

5. Illustrative examples

In this section, the proposed design approach is demonstrated through two examples comparing the advantages of using a QPDLF versus the LMI methodology proposed in [19], where a constant quadratic Lyapunov function (QLF) was used. Section 5.1 presents a numerical example where the influence of the saturation limit variation range and the bounds of $\dot{\eta}_j(\varphi)$ is shown. Then, Section 5.2 shows the closed-loop response of the attitude control of a quadrotor with a performance that varies online according to the value of the instantaneous saturation limits given by the maximum angular rotor speed.

The simulations are obtained in *MATLAB* environment, by implementing Theorem 3 via the *YALMIP* toolbox [34] using the solver *SeDuMi* [35]. Additionally, the *Multi-Parametric Toolbox 3.0* (MPT3) [36] was used in both examples in order to obtain a finite number of vectors (34)–(35) by solving a vertex enumeration problem through the function *Polyhedron*, whose input arguments are $\bar{A}$, b, A_e and b_e. These arguments can be obtained by expressing the constraints (8) and (32) in the form of $\bar{A}x \leq b$ and $A_e x \leq b_e$ as follows:

$$\begin{aligned} \bar{A} &= I_N \otimes \begin{bmatrix} 1 \\ -1 \end{bmatrix}, \quad b = \begin{bmatrix} \overline{v}_1 \\ -\underline{v}_1 \\ \vdots \\ \overline{v}_N \\ -\underline{v}_N \end{bmatrix}, \\ A_e &= \underbrace{\begin{bmatrix} 1 & 1 & \ldots & 1 \end{bmatrix}}_{N} \quad b_e = 0, \end{aligned} \tag{51}$$

and similarly for the constraints (10) and (33).

For both examples, the polytopic weights $\mu_i(\vartheta)$ were obtained by means of the simplest polytopic approximation, known as *bounding box*, which relies on bounding each scheduling parameter of ϑ by an interval [31]. Similarly, $\eta_j(\varphi)$ were obtained applying the same approach except for Section 5.2, where a less conservative approach was used, as described therein.

5.1. Example 1: Numerical example

Consider an open-loop unstable LPV system modelled as in (3), $\vartheta(t) \in [0, 1]$ and the following state-space matrices:

$$A(\vartheta(t)) = \begin{bmatrix} 4.25 + 3.5\vartheta(t) & 3.8971 \\ 3.8971 & 8.75 - 5.5\vartheta(t) \end{bmatrix} \quad B = \begin{bmatrix} 1 & 0 \\ 0 & 0.5 \end{bmatrix}, \tag{52}$$

where the parameter-dependent matrix $A(\vartheta(t))$ and the matrix B can be written in polytopic form by means of the Definition 1, assuming that B has the same value for all the $N = 2$ vertices:

$$A_1 = \begin{bmatrix} 4.25 & 3.8971 \\ 3.8971 & 8.75 \end{bmatrix}, \quad A_2 = \begin{bmatrix} 7.75 & 3.8971 \\ 3.8971 & 3.25 \end{bmatrix}. \tag{53}$$

Table 1
Experiment specifications for Example 1. (d, s Pólya's relaxation degree; X_0 magnitudes of (17); $\dot{\mu}_i(\vartheta)$, $\dot{\eta}_j(\varphi)$ time-derivative polytopic weights limits (8) and (10).)

Scenario	d	s	X_0	$\dot{\mu}_i(\vartheta)\ \forall i = 1, 2$	$\dot{\eta}_j(\varphi)\ \forall j = 1, 2$
A	2	–	$diag(100, 100)$	–	–
B	2	2	$diag(100, 100)$	$[-1, 1]$	$[-1, 1]$
C	2	2	$diag(100, 100)$	$[-1, 1]$	$[-5, 5]$
D	2	2	$diag(100, 100)$	$[-1, 1]$	$[-10, 10]$

Table 2
Expected initial conditions for Euler angles in Example 2. ($\underline{\xi}_\kappa$ and $\overline{\xi}_\kappa$ denote the lower and upper bound value expressed in [rad], respectively.)

κ	$[\underline{\xi}_\kappa,\ \overline{\xi}_\kappa]$
1	$[-0.0087,\ 0.0087]$
2	$[-0.0436,\ 0.0436]$
3	$[-0.0873,\ 0.0873]$
4	$[-0.1309,\ 0.1309]$
5	$[-0.1745,\ 0.1745]$

5.1.1. Time-varying saturation limits definition

Let us define the time-varying saturation for the inputs $u_1(t)$ and $u_2(t)$ as follows:

$$sat(u_h(t), \sigma_h(t)) = sign(u_h(t)) \min(|u_h(t)|, \sigma_h(t)) \quad h = 1, 2, \tag{54}$$

where $\sigma_1(t)$ varies within the interval $[5, \overline{\sigma}_1]$ and $\sigma_2(t) = \sigma_2 = 5$. Thereupon, let us introduce the scheduling parameter $\varphi(t)$, which is linked to $\sigma_1(t)$ as follows:

$$\varphi(t) = \frac{\sigma_1(t)^2 - 25}{\overline{\sigma}_1^2 - 25}, \tag{55}$$

so that $\varphi(t) \in [0, 1]$. Moreover, note that (55) allows us expressing $\sigma_1(t)^2$ as a function of $\varphi(t)$:

$$\sigma_1(\varphi(t))^2 = 25 + \varphi(t)(\overline{\sigma}_1^2 - 25). \tag{56}$$

Then, assuming that the control inputs are aligned with the axis of the hyper-ellipsoidal region $\mathcal{U}(\varphi(t))$ (14), the matrix function $S(\varphi(t))$ is described as follows:

$$S(\varphi(t)) = diag(\sigma_1(\varphi(t))^2,\ 25)^{-1} \tag{57}$$

and the corresponding vertex matrices are

$$S_1 = \begin{bmatrix} \frac{1}{25} & 0 \\ 0 & \frac{1}{25} \end{bmatrix}, \quad S_2 = \begin{bmatrix} \frac{1}{\overline{\sigma}_1^2} & 0 \\ 0 & \frac{1}{25} \end{bmatrix}. \tag{58}$$

5.1.2. Methodology comparison

Let us establish the following set conditions with the purpose of evaluating the advantage of using the QPDLF (12) instead of a QLF. To this end, $\overline{\sigma}_1$ and the maximum desired decay rate value $\overline{\lambda}$ are generated as follows:

$$\overline{\sigma}_1 \triangleq \{n \in \mathbb{R}_+ : 5 < n \leq 105\}, \quad \overline{\lambda} \triangleq \{n \in \mathbb{R}_+ : 0 \leq n \leq 100\}.$$

Furthermore, the desired vertex values of (28) are fixed to

$$\lambda_{i1} = 0,\ \lambda_{i2} = \overline{\lambda}\ \forall i = 1, 2,$$

where λ_{i2} will be evaluated for each combination of the selected values of $\overline{\sigma}_1$ and $\overline{\lambda}$.

Table 1 shows the selected specifications for the different established scenarios. Scenario **A** corresponds to use the QLF defined in [19], whereas Scenarios **B-D** correspond to use the QPDLF defined as in (12) and the polytopic representations (30) and (38).

Finally, Theorem 3 is evaluated for each element of $\overline{\sigma}_1$ and $\overline{\lambda}$ under the different scenarios described in Table 1. Fig. 1 shows, for each fixed value of $\overline{\sigma}_1$, the maximum value obtained for $\overline{\lambda}$ so that the set of LMIs (39) and (42)–(43) described in Theorem 3 is feasible. The benefits of using a QPDLF instead of using a QLF can be observed, as a larger feasible guaranteed decay rate is obtained when a larger range of variation of $\sigma_1(t)$ is considered. However, note that for small variations of $\sigma_1(t)$, the maximum feasible values of $\overline{\lambda}$ are practically the same for both cases. Furthermore, when large bounds are considered for $\dot{\eta}_j(\varphi)$, the QLF approach and the proposed QPDLF approach provide similar performance for big values of $\overline{\sigma}_1$.

5.2. Example 2: Attitude control of a quadrotor

Consider the attitude model of a quadrotor borrowed from [37] with parameters as described in [38]. The state vector $x(t) = [\phi, \dot{\phi}, \theta, \dot{\theta}, \psi, \dot{\psi}]^T$ is constructed with the Euler angles $\phi(t)$–roll, $\theta(t)$–pitch, $\psi(t)$–yaw and the Euler angle rates $\dot{\phi}(t)$, $\dot{\theta}(t)$ and $\dot{\psi}(t)$. The input vector $u(t) = [u_1(t), u_2(t), u_3(t)]^T$ contains the moments produced by the rotors as follows:

$$\begin{aligned} u_1(t) &= k_T l(\Omega_4^2(t) - \Omega_2^2(t)) \\ u_2(t) &= k_T l(\Omega_1^2(t) - \Omega_3^2(t)) \\ u_3(t) &= k_Q(-\Omega_1^2(t) + \Omega_2^2(t) - \Omega_3^2(t) + \Omega_4^2(t)) \end{aligned}, \tag{59}$$

where l is the distance expressed in metres from the centre of gravity (CoG) of the corresponding rotor to the quadrotor's CoG, k_T denotes the thrust coefficient expressed in [N/rpm^2] and k_Q corresponds to the torque coefficient in [N m/rpm^2]. $\Omega_i(t)$ denotes the angular speed of the ith propeller in [rpm].

Thereupon, the parameter scheduling vector $\vartheta(t) = [\dot{\phi}(t), \dot{\theta}(t), \Omega_r(t)]$ is constructed[2] by the Euler angle rates $\dot{\phi}(t) \in [-1, 1]$ [rad/s] and $\dot{\theta}(t) \in [-1, 1]$ [rad/s], and the gyroscopic effect $\Omega_r(t) \in [-105, 105]$ [rad/s] which is characterized as follows:

$$\Omega_r(t) = \frac{\pi}{30}(\Omega_1(t) + \Omega_3(t) - \Omega_2(t) - \Omega_4(t)). \tag{60}$$

In this way, the polytope Θ is a cube with $N = 8$ vertices and the following parameter-dependent state-matrices:

$$A(\vartheta(t)) = \begin{bmatrix} 0 & 1 & 0 & 0 & 0 & 0 \\ 0 & 0 & 0 & a_{24}(\cdot) & 0 & a_{26}(\cdot) \\ 0 & 0 & 0 & 1 & 0 & 0 \\ 0 & a_{42}(\cdot) & 0 & 0 & 0 & a_{46}(\cdot) \\ 0 & 0 & 0 & 0 & 0 & 1 \\ 0 & a_{62}(\cdot) & 0 & a_{64}(\cdot) & 0 & 0 \end{bmatrix},$$
$$B = \begin{bmatrix} 0 & 0 & 0 \\ \frac{1}{J_x} & 0 & 0 \\ 0 & 0 & 0 \\ 0 & \frac{1}{J_y} & 0 \\ 0 & 0 & 0 \\ 0 & 0 & \frac{1}{J_z} \end{bmatrix}, \tag{61}$$

where $a_{24}(\vartheta_3(t)) = -\vartheta_3(t)\frac{J_{tp}}{J_x}$, $a_{26}(\vartheta_2(t)) = \vartheta_2(t)\frac{J_y - J_z}{J_x}$, $a_{42}(\vartheta_3(t)) = \vartheta_3(t)\frac{J_{tp}}{J_x}$, $a_{46}(\vartheta_1(t)) = \vartheta_1(t)\frac{J_z - J_x}{J_y}$, $a_{62}(\vartheta_2(t)) = \frac{\vartheta_2(t)}{2}\frac{J_x - J_y}{J_z}$ and $a_{64}(\vartheta_1(t)) = \frac{\vartheta_1(t)}{2}\frac{J_x - J_y}{J_z}$. The symbols J_{tp}, J_x, J_y, J_z correspond to the total rotational moment of inertia around propeller axis and the body moment of inertia around the $x, y, z - axis$ expressed in [kg m^2], respectively.

Consider that the angular speed of each propeller Ω_i varies within the same interval $[\underline{\Omega}, \overline{\Omega}(t)]\ \forall i = 1, \ldots, 4$. The symbol $\underline{\Omega}$ corresponds to the minimum propeller angular speed, fixed

[2] Note that the obtained model is *quasi-LPV* due to the dependence of the scheduling vector on endogenous variables.

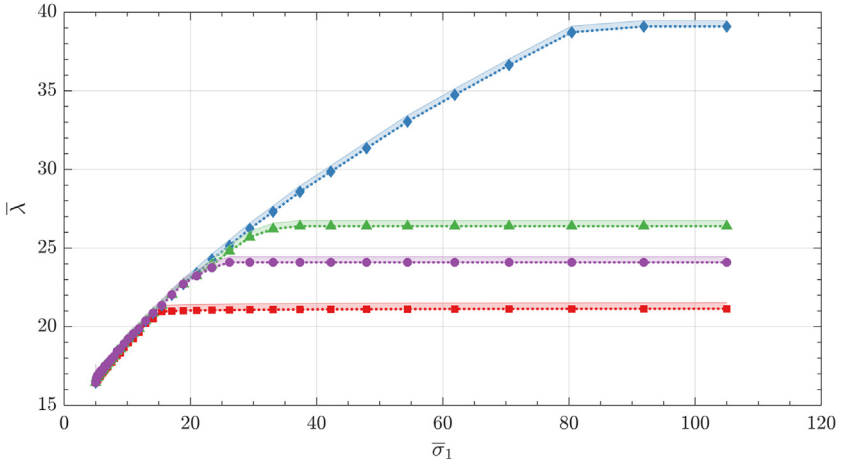

Fig. 1. Results of applying Theorem 3 in the numerical system (52). (The following symbols denote the selected scenarios: **A**; **B**; **C**; and **D**.)

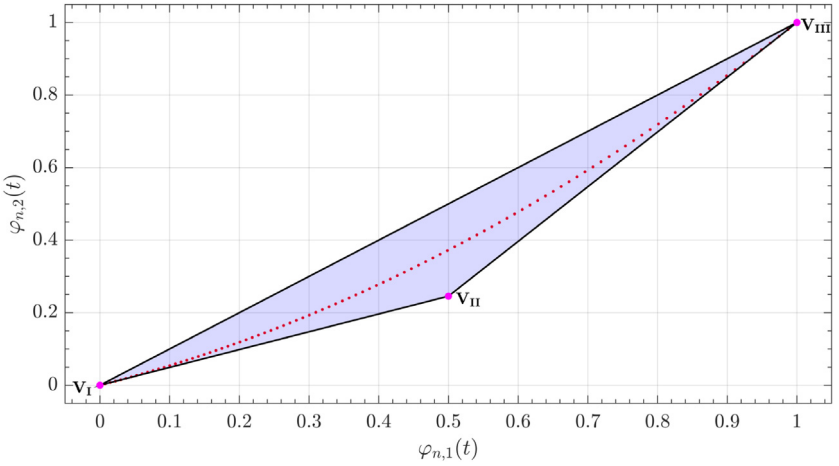

Fig. 2. Polytope Φ. (• denotes the normalized values of $\varphi_{n,1}(t)$ and $\varphi_{n,2}(t)$; • denotes the polytope vertices).

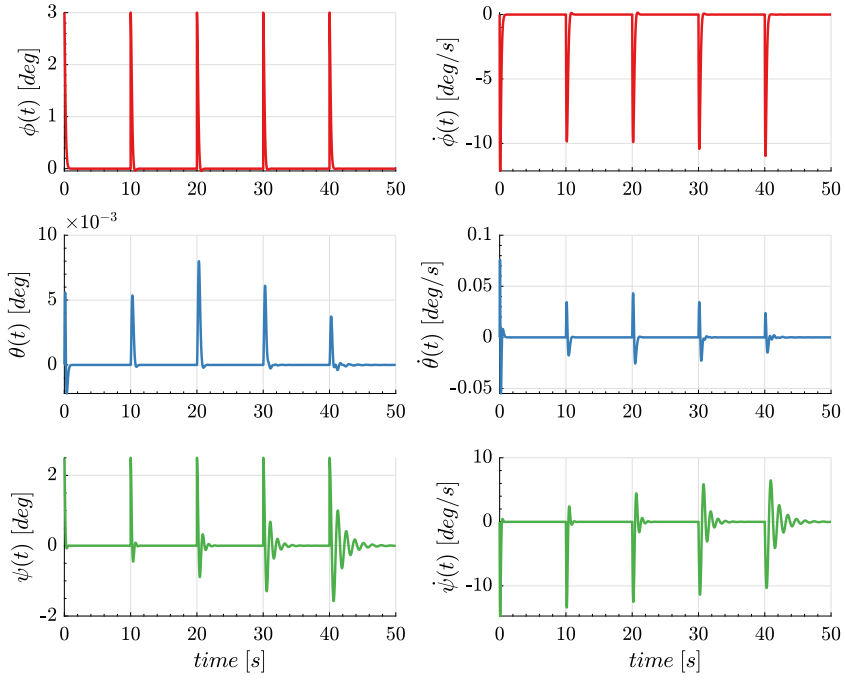

Fig. 3. Quadrotor's attitude closed-loop response.

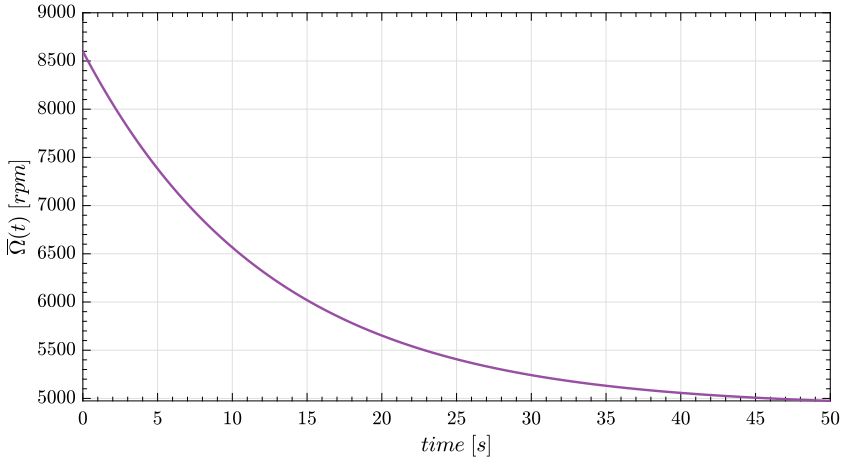

Fig. 4. Maximum propeller speed due to the battery discharge.

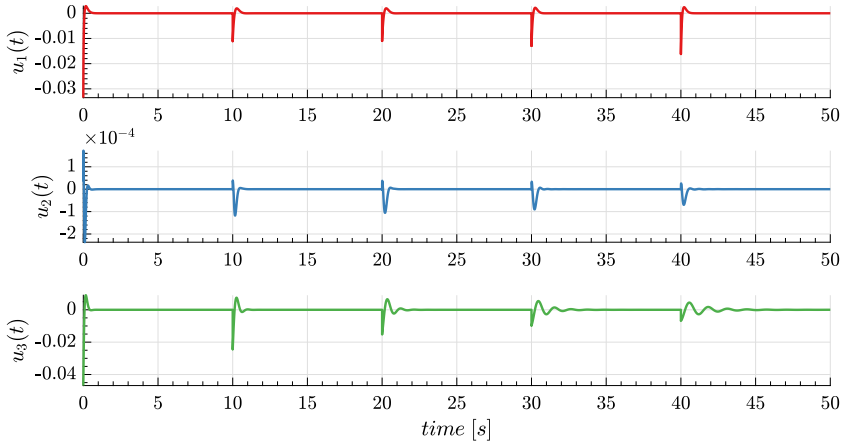

Fig. 5. Quadrotor's attitude control actions.

to 1075 [rpm]. Then, let us assume that the function $\overline{\Omega}(t)$ is known and that it describes how the maximum propeller angular speed decreases over time due to the discharge of the battery. To this end, $\overline{\Omega}(t)$ is considered as the instantaneous value of the maximum propeller angular speed, and it is assumed to vary within the interval [4907, 8600] [rpm].

5.2.1. Time-varying saturation limits definition

In order to handle the propeller speed limitation, let us define the time-varying saturation for $u(t)$ as follows:

$$sat(u_h(t), \sigma_h(t)) = sign(u_h(t)) \min(|u_h(t)|, \sigma_h(t)) \quad h = 1, 2, 3, \tag{62}$$

where $\sigma_1(t)$, $\sigma_2(t)$ and $\sigma_3(t)$ are defined as the largest available positive control action through Eq. (59) and the function $\overline{\Omega}(t)$ as follows:

$$\begin{aligned} \sigma_1(t) &= \sigma_2(t) = k_T l(\overline{\Omega}(t)^2 - \underline{\Omega}^2) \\ \sigma_3(t) &= 2k_Q(\overline{\Omega}(t)^2 - \underline{\Omega}^2). \end{aligned} \tag{63}$$

Similarly to Section 5.1, let us assume that the axes of $u(t)$ are aligned with the axes of the hyper-ellipsoidal region $\mathcal{U}(\varphi(t))$ (14). Then, let us define the squared expression of Eq. (63) as follows

$$\begin{aligned} \sigma_1(t)^2 &= \sigma_2(t)^2 = k_T^2 l^2(\overline{\Omega}(t)^4 - 2\overline{\Omega}(t)^2\underline{\Omega}^2 + \underline{\Omega}^4) \\ \sigma_3(t)^2 &= 4k_Q^2(\overline{\Omega}(t)^4 - 2\overline{\Omega}(t)^2\underline{\Omega}^2 + \underline{\Omega}^4). \end{aligned} \tag{64}$$

Thereupon, let us introduce the following scheduling parameters $\varphi_1(t)$ and $\varphi_2(t)$ which are linked to $\overline{\Omega}(t)^2$ and $\overline{\Omega}(t)^4$, respectively, thus obtaining expressions of $\sigma_1(t)^2$, $\sigma_2(t)^2$ and $\sigma_3(t)^2$ as a function of $\varphi(t) = [\varphi_1(t), \varphi_2(t)]^T$:

$$\begin{aligned} \sigma_1(\varphi(t))^2 &= \sigma_2(\varphi(t))^2 = k_T^2 l^2(\varphi_2(t) - 2\varphi_1(t)\underline{\Omega}^2 + \underline{\Omega}^4) \\ \sigma_3(\varphi(t))^2 &= 4k_Q^2(\varphi_2(t) - 2\varphi_1(t)\underline{\Omega}^2 + \underline{\Omega}^4). \end{aligned} \tag{65}$$

Once Eq. (65) is obtained, the axis magnitudes of $\mathcal{U}(\varphi(t))$ are established through the matrix function $S(\varphi(t))$ as follows:

$$S(\varphi(t)) = diag(\sigma_1(\varphi(t))^2, \sigma_2(\varphi(t))^2, \sigma_3(\varphi(t))^2)^{-1}. \tag{66}$$

For the purpose of solving Problem 1, let us define the polytope Φ (where the scheduling parameters $\varphi_1(t)$ and $\varphi_2(t)$ lie) generating a set of possible values for both parameters taking into account the bounds of $\overline{\Omega}(t)$. Note that these sets reach large values due to $\varphi_1(t)$ and $\varphi_2(t)$ being linked to square and fourth power of $\overline{\Omega}(t)$, respectively. Hence, it is necessary to normalize both parameters in the range [0, 1] in order to avoid numerical issues when computing $\eta_j(\varphi(t))$.

Fig. 2 shows the generated values for the normalized parameters $\varphi_{n,1}(t)$ and $\varphi_{n,2}(t)$ as well as the selected $M = 3$ vertices $\mathbb{V}_{\mathrm{I}} = [0, 0]$, $\mathbb{V}_{\mathrm{II}} = [0.5, 0.2456]$ and $\mathbb{V}_{\mathrm{III}} = [1, 1]$ that define the polytope Φ.

Then, taking into account the bounds of the polytope Φ, it is possible to compute $\eta_j(\varphi(t))$ $\forall j = 1, 2, 3$ as the solution of the

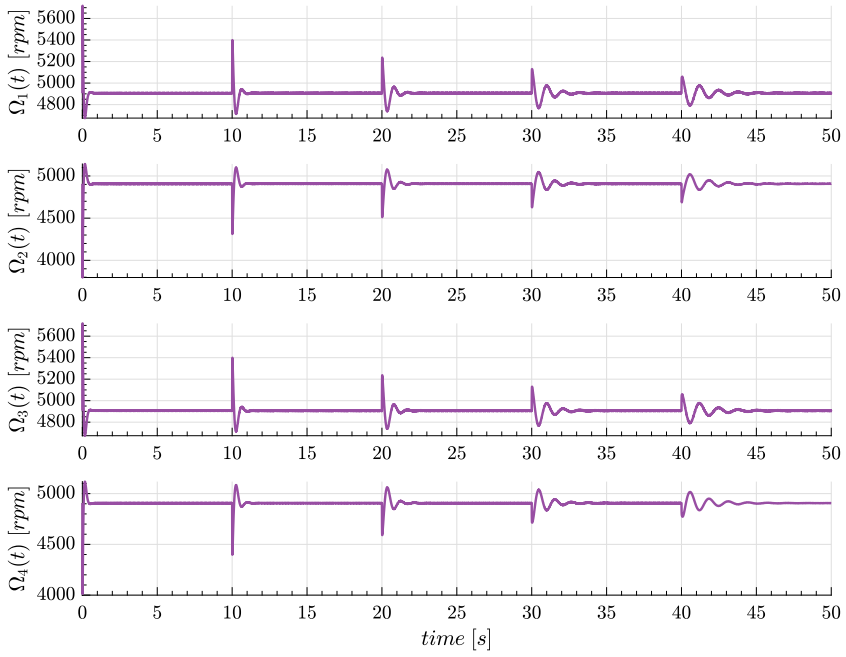

Fig. 6. Propellers' angular speed.

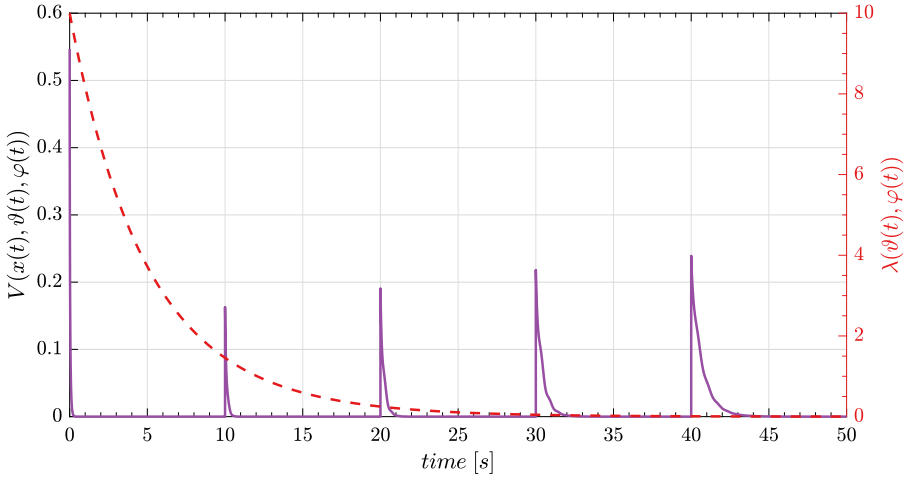

Fig. 7. QPDLF and guaranteed shifting decay rate. (— corresponds to $V(x(t), \vartheta(t), \varphi(t))$; - - denotes $\lambda(\vartheta(t), \varphi(t))$).

following equation:

$$\begin{bmatrix} \varphi_{n,1}(t) \\ \varphi_{n,2}(t) \\ 1 \end{bmatrix} = \begin{bmatrix} \mathbb{V}_{\mathrm{I},1} & \mathbb{V}_{\mathrm{II},1} & \mathbb{V}_{\mathrm{III},1} \\ \mathbb{V}_{\mathrm{I},2} & \mathbb{V}_{\mathrm{II},2} & \mathbb{V}_{\mathrm{III},2} \\ 1 & 1 & 1 \end{bmatrix} \begin{bmatrix} \eta_1(\varphi(t)) \\ \eta_2(\varphi(t)) \\ \eta_3(\varphi(t)) \end{bmatrix}. \tag{67}$$

5.2.2. Methodology comparison

Let us now describe the performance specifications for the controller design considering that the initial state of the quadrotor is around the hover attitude point ($\phi(t) = 0$, $\theta(t) = 0$) with the purpose of evaluating the LMI methodology described in Theorem 3 versus the procedure proposed in [19] under the scenarios indicated in Table 2.

To this end, let us define the shape of the region (17) considering that the initial attitude of the vehicle $\phi(0)$, $\theta(0)$ and $\psi(0)$ belongs to the interval $[\underline{\xi}_\kappa, \overline{\xi}_\kappa]$ expressed in [rad] for each scenario κ. Furthermore, each initial value of the Euler angle rates $\dot{\phi}(0)$, $\dot{\theta}(0)$ and $\dot{\psi}(0)$ is expected to be inside the interval $[-0.3491, 0.3491]$ [rad/s], thus specifying:

$$X_0 = diag(\overline{\xi}_\kappa,\ 0.3491,\ \overline{\xi}_\kappa,\ 0.3491,\ \overline{\xi}_\kappa,\ 0.3491)^{-2},$$

where $\overline{\xi}_\kappa$ denotes the corresponding κ upper bound value of the interval.

Table 3
Maximum feasible values of $\lambda_{i,3}$. (Δ denotes the improvement in percentage with respect to the value obtained through the Theorem 2 [19].)

κ	Theorem 2 [19]	Theorem 3	Δ (%)
1	19.27	26.46	37.31
2	10.70	14.13	32.06
3	7.67	10.03	30.77
4	6.15	7.56	22.93
5	5.65	7.07	25.13

Table 4
Off-line computational cost.

	Theorem 2 [19]	Theorem 3
Number of LMIs	134	90 792
Computation time[a] [s]	0.7126	19 134

[a]4 cores 2.80 GHz CPU with 16 GB RAM.

Then, with the aim of controlling online the convergence speed of the closed-loop system, let us define the desired decay rate values in (28) as follows:

$$\lambda_{i1} = 0,\ \lambda_{i2} = 0,\ \lambda_{i3} = \overline{\lambda} \quad \forall i = 1, \ldots, 8,$$

thus specifying the fastest closed-loop system response when the largest saturation limit of $u(t)$ is available.

Once the performance specifications are defined, let us proceed to compare Theorem 3 against Theorem 2 in [19] by evaluating $\overline{\lambda}$ for each value of the set $\{n \in \mathbb{R}_+ : 0 \leq n \leq 100\}$. Thus, obtaining the maximum feasible decay rate $\overline{\lambda}$ shown in Table 3 for each scenario κ under the consideration of choosing the Pólya's relaxation degrees $d = s = 2$, the bounds of (8) $\forall i = 1, \ldots, 8$ as $[-0.8, 0.8]$ and, similarly, the bounds in (10) are established $\forall j = 1, 2, 3$ as $[-0.05, 0.05]$.

The benefits of using Theorem 3 instead of using the procedure proposed in [19] can be observed in Table 3, as an improvement of 20–30% with respect to the largest feasible guaranteed decay rate obtained when QLF is used for the above defined conditions. However, this improvement comes at the cost of increasing significantly the computational cost, as shown in Table 4. Note that the increase in computational burden affects only the off-line computation due to the growth of the number of LMIs that must be satisfied. On the other hand, the online computation is not affected, since the total number of vertices does not depend on which of the methodologies is used.

5.2.3. Closed-loop response

Let us show how the performance varies online according to the value of the instantaneous saturation limits given by $\overline{\Omega}(t)$ through the results shown in Figs. 3–7 which correspond to the controller designed under the initial conditions of scenario $\kappa = 3$ and guaranteed decay rates: $\lambda_{i,1} = 0$, $\lambda_{i,2} = 0$, and $\lambda_{i,3} = 10.0$ $\forall i = 1, \ldots, 8$.

As shown in Fig. 3, the closed-loop system stability is guaranteed $\forall t \geq 0$. Moreover, note that jumps in the values of $\phi(t)$ and $\psi(t)$ were introduced every 10 s in order to show the effectiveness of the controller. It can be seen that the slowest system response corresponds to when $\overline{\Omega}(t) \to \underline{\Omega}$ at $t \geq 30$, as shown in Fig. 4. Conversely, the fastest closed-loop response corresponds to when the maximum angular speed of each propeller is available. This demonstrates that the designed shifting LPV state-feedback controller adapts online the closed-loop system response in the sense of convergence speed according to the available control action.

Fig. 4 shows the evolution of the maximum available propeller angular speed, which decreases its value over time reproducing an incipient discharge of the battery, which limits the instantaneous value of $u(t)$ according to (63). This fact is exemplified in Fig. 5, where smaller values of $u(t)$ were obtained over time preventing saturation to occur. Similarly, Fig. 6 shows the behaviour of the angular speed for each propeller under the scenario described above.

Finally, Fig. 7 shows the adaptability of the control performance through the evolution of the QPDLF (12). Note that the largest value of $\lambda(\vartheta(t), \varphi(t))$ stands for the fastest closed-loop response showed in Fig. 3, whose instantaneous saturation limits corresponded to the largest possible ones. Furthermore, $V(x(t), \vartheta(t), \varphi(t))$ is under the unit value $\forall t \geq 0$, which provides theoretical guarantees that none of the control actions saturates during the transient response, as already shown in Fig. 5.

6. Conclusions

In this work, we have considered the issues of designing a shifting LPV state-feedback controller via QPDLFs for LPV systems subject to time-varying input saturation limits. The design procedure proposed in [19] has been extended through the use of a QPDLF obtaining a suitable set of LMIs, which can be accurately solved with accessible solvers. Furthermore, Pólya's theorem has been used in order to deal with the multiple polytopic summations, reducing the complexity in the design stage.

The results obtained in the illustrative examples have shown the improvements and the effectiveness brought by the proposed approach. The designed controller has shown its ability to regulate the closed-loop system convergence speed according to the instantaneous saturation limit values of the actuators. The results obtained so far appear to be less conservative, although at the cost of increasing the computational burden and the mathematical complexity, which could hinder the implementation of the proposed design approach in higher-order plants due to the large number of required LMIs. Future research will aim at reducing the computational complexity by focusing on the application of hybrid techniques (for example, MPC with LPV, or feedback linearization with LPV) or more advanced LPV frameworks which incorporate switching elements, in order to reduce the number of LMIs to be handled.

Declaration of competing interest

The authors declare that they have no known competing financial interests or personal relationships that could have appeared to influence the work reported in this paper.

Acknowledgements

This work has been partially funded by the Spanish State Research Agency (AEI) and the European Regional Development Fund (ERFD) through the project SaCoAV (ref. PID2020-114244RB-I00). This work has also been partially funded by AGAUR of Generalitat de Catalunya, Spain through the Advanced Control Systems (SAC) group grant (2017 SGR 482) and by the University of Stavanger, Norway through the project IN-12267. A. Ruiz is also supported by the Secretaria d'Universitats i Recerca de la Generalitat de Catalunya, Spain, the European Social Fund (ESF) and AGAUR under a FI SDUR grant (ref. 2020 FI-SDUR 00097).

Appendix

A.1. Proof of Theorem 2

Proof of Theorem 2. Let us take into account the polytopic representation of matrices $A(\vartheta)$ and $B(\vartheta)$ as in (7), so that the parameter-dependent LMI (20) is equivalent to:

$$He\left\{\sum_{a=1}^{N} \mu_a(\vartheta) A_a Q(\vartheta, \varphi) + \sum_{b=1}^{N} \mu_b(\vartheta) B_b \Gamma(\vartheta, \varphi)\right\} + 2\lambda(\vartheta, \varphi) Q(\vartheta, \varphi) - \dot{Q}(\vartheta, \varphi) \preceq 0. \tag{A.1}$$

Then, let us take into account the polytopic representation of $\lambda(\vartheta,\varphi)$, $\Gamma(\vartheta,\varphi)$ and $Q(\vartheta,\varphi)$ given in (28)–(30), thus obtaining:

$$\begin{aligned} He\Bigg\{ &\sum_{a=1}^{N}\sum_{b=1}^{N}\sum_{c=1}^{M}\mu_a(\vartheta)\mu_b(\vartheta)\eta_c(\varphi)A_aQ_{bc} \\ &+\sum_{a=1}^{N}\sum_{b=1}^{N}\sum_{c=1}^{M}\mu_b(\vartheta)\mu_a(\vartheta)\eta_c(\varphi)B_b\Gamma_{ac}\Bigg\} \\ &+2\sum_{a=1}^{N}\sum_{b=1}^{N}\sum_{c=1}^{M}\sum_{d=1}^{M}\mu_a(\vartheta)\mu_b(\vartheta)\eta_c(\varphi)\eta_d(\varphi)\lambda_{ac}Q_{bd} \\ &-\dot{Q}(\vartheta,\varphi)\preceq 0. \end{aligned} \tag{A.2}$$

Right after, let us replace $\dot{Q}(\vartheta,\varphi)$ in Eq. (A.2) by the expression given in (38), as follows:

$$\begin{aligned} He\Bigg\{ &\sum_{a=1}^{N}\sum_{b=1}^{N}\sum_{c=1}^{M}\mu_a(\vartheta)\mu_b(\vartheta)\eta_c(\varphi)A_aQ_{bc} \\ &+\sum_{a=1}^{N}\sum_{b=1}^{N}\sum_{c=1}^{M}\mu_b(\vartheta)\mu_a(\vartheta)\eta_c(\varphi)B_b\Gamma_{ac}\Bigg\} \\ &+2\sum_{a=1}^{N}\sum_{b=1}^{N}\sum_{c=1}^{M}\sum_{d=1}^{M}\mu_a(\vartheta)\mu_b(\vartheta)\eta_c(\varphi)\eta_d(\varphi)\lambda_{ac}Q_{bd} \\ &-\sum_{m=1}^{N}\sum_{c=1}^{M}\sum_{k=1}^{O}\alpha_k(\vartheta,\dot{\vartheta})\eta_c(\varphi)f_m^{\{k\}}Q_{mc} \\ &-\sum_{a=1}^{N}\sum_{n=1}^{M}\sum_{l=1}^{R}\mu_a(\vartheta)\beta_l(\varphi,\dot{\varphi})g_n^{\{l\}}Q_{an}\preceq 0, \end{aligned} \tag{A.3}$$

which can be rewritten taking into account that the coefficients appearing in Eq. (A.3) sum to one, see (7), (9), (36) and (37), thus obtaining:

$$\begin{aligned} He\Bigg\{ &\sum_{a=1}^{N}\sum_{b=1}^{N}\sum_{c=1}^{M}\sum_{d=1}^{M}\sum_{k=1}^{O}\sum_{l=1}^{R}\mu_a(\vartheta)\mu_b(\vartheta)\eta_c(\varphi)\eta_d(\varphi)\alpha_k(\vartheta,\dot{\vartheta}) \\ &\times\beta_l(\varphi,\dot{\varphi})A_aQ_{bc} \\ &+\sum_{a=1}^{N}\sum_{b=1}^{N}\sum_{c=1}^{M}\sum_{d=1}^{M}\sum_{k=1}^{O}\sum_{l=1}^{R}\mu_b(\vartheta)\mu_a(\vartheta)\eta_c(\varphi)\eta_d(\varphi)\alpha_k(\vartheta,\dot{\vartheta}) \\ &\times\beta_l(\varphi,\dot{\varphi})B_b\Gamma_{ac}\Bigg\} \\ &+2\sum_{a=1}^{N}\sum_{b=1}^{N}\sum_{c=1}^{M}\sum_{d=1}^{M}\sum_{k=1}^{O}\sum_{l=1}^{R}\mu_a(\vartheta)\mu_b(\vartheta)\eta_c(\varphi)\eta_d(\varphi)\alpha_k(\vartheta,\dot{\vartheta}) \\ &\times\beta_l(\varphi,\dot{\varphi})\lambda_{ac}Q_{bd} \\ &-\sum_{a=1}^{N}\sum_{b=1}^{N}\sum_{m=1}^{N}\sum_{c=1}^{M}\sum_{d=1}^{M}\sum_{k=1}^{O}\sum_{l=1}^{R}\mu_a(\vartheta)\mu_b(\vartheta)\eta_c(\varphi)\eta_d(\varphi)\alpha_k(\vartheta,\dot{\vartheta}) \\ &\times\beta_l(\varphi,\dot{\varphi})f_m^{\{k\}}Q_{mc} \\ &-\sum_{a=1}^{N}\sum_{b=1}^{N}\sum_{c=1}^{M}\sum_{d=1}^{M}\sum_{n=1}^{M}\sum_{k=1}^{O}\sum_{l=1}^{R}\mu_a(\vartheta)\mu_b(\vartheta)\eta_c(\varphi)\eta_d(\varphi)\alpha_k(\vartheta,\dot{\vartheta}) \\ &\times\beta_l(\varphi,\dot{\varphi})g_n^{\{l\}}Q_{an}\preceq 0. \end{aligned} \tag{A.4}$$

The following Eq. (A.5) is obtained from Eq. (A.4) through the application of the common factor:

$$\begin{aligned} &\sum_{a=1}^{N}\sum_{b=1}^{N}\sum_{c=1}^{M}\sum_{d=1}^{M}\sum_{k=1}^{O}\sum_{l=1}^{R}\mu_a(\vartheta)\mu_b(\vartheta)\eta_c(\varphi)\eta_d(\varphi)\alpha_k(\vartheta,\dot{\vartheta}) \\ &\times\beta_l(\varphi,\dot{\varphi}) \\ &\left[He\left\{A_aQ_{bc}+B_b\Gamma_{ac}\right\}+2\lambda_{ac}Q_{bd}-\sum_{m=1}^{N}f_m^{\{k\}}Q_{mc}-\sum_{n=1}^{M}g_n^{\{l\}}Q_{an}\right]\preceq 0. \end{aligned} \tag{A.5}$$

By applying *Pólya's theorem* on the definiteness of quadratic forms involving multiple summations [29], the set of LMIs in (39) is obtained, thus concluding the proof. ■

References

[1] Kapila V, Grigoriadis K. Actuator saturation control. CRC Press; 2002.
[2] Tarbouriech S, Garcia G, da Silva Jr JMG, Queinnec I. Stability and stabilization of linear systems with saturating actuators. Springer Science & Business Media; 2011.
[3] Corradini ML, Cristofaro A, Giannoni F, Orlando G. Control systems with saturating inputs: Analysis tools and advanced design, Vol. 424. Springer Science & Business Media; 2012.
[4] Tahoun A. Anti-windup adaptive PID control design for a class of uncertain chaotic systems with input saturation. ISA Trans 2017;66:176–84.
[5] Hu T, Teel AR, Zaccarian L. Anti-windup synthesis for linear control systems with input saturation: Achieving regional, nonlinear performance. Automatica 2008;44(2):512–9.
[6] Da Silva JG, Tarbouriech S. Local stabilization of discrete-time linear systems with saturating controls: an LMI-based approach. IEEE Trans Automat Control 2001;46(1):119–25.
[7] Aouaouda S, Chadli M. Robust fault tolerant controller design for takagi-sugeno systems under input saturation. Internat J Systems Sci 2019;50(6):1163–78.
[8] Hoffmann C, Werner H. A survey of linear parameter-varying control applications validated by experiments or high-fidelity simulations. IEEE Trans Control Syst Technol 2014;23(2):416–33.
[9] Shamma JS. Analysis and design of gain scheduled control systems (Ph.D.thesis), Massachusetts Institute of Technology; 1988.
[10] White AP, Zhu G, Choi J. Linear parameter-varying control for engineering applications. Springerbriefs in electrical and computer engineering, London: Springer London; 2013, http://dx.doi.org/10.1007/978-1-4471-5040-4.
[11] Bianchi FD, Mantz RJ, Christiansen CF. Gain scheduling control of variable-speed wind energy conversion systems using quasi-LPV models. Control Eng Pract 2005;13(2):247–55.
[12] Morato MM, Nguyen MQ, Sename O, Dugard L. Design of a fast real-time LPV model predictive control system for semi-active suspension control of a full vehicle. J Franklin Inst B 2019;356(3):1196–224. http://dx.doi.org/10.1016/j.jfranklin.2018.11.016.
[13] Karimi Pour F, Theilliol D, c Puig V, Cembrano G. Health-aware control design based on remaining useful life estimation for autonomous racing vehicle. ISA Trans 2020. http://dx.doi.org/10.1016/j.isatra.2020.03.032.
[14] Cao Y-Y, Lin Z. Min–max MPC algorithm for LPV systems subject to input saturation. IEEE Proc D 2005;152(3):266–72.
[15] Wu F, Grigoriadis KM, Packard A. Anti-windup controller design using linear parameter-varying control methods. Internat J Control 2000;73(12):1104–14.
[16] Dabiri A, Kulcsár B, Köroğlu H. Distributed LPV state-feedback control under control input saturation. IEEE Trans Automat Control 2016;62(5):2450–6.
[17] Podhradský M, Bone J, Coopmans C, Jensen A. Battery model-based thrust controller for a small, low cost multirotor unmanned aerial vehicles. In: 2013 international conference on unmanned aircraft systems (ICUAS). 2013, p. 105–13. http://dx.doi.org/10.1109/ICUAS.2013.6564679.
[18] Bouabdallah S, Siegwart R. Full control of a quadrotor. In: 2007 IEEE/RSJ international conference on intelligent robots and systems. 2007, p. 153–8. http://dx.doi.org/10.1109/IROS.2007.4399042.
[19] Ruiz A, Rotondo D, Morcego B. Design of state-feedback controllers for linear parameter varying systems subject to time-varying input saturation. Appl Sci 2019;9(17):3606.
[20] Ruiz A, Rotondo D, Morcego B. Shifting $\mathcal{H}_\infty$ linear parameter varying state-feedback controllers subject to time-varying input saturations. IFAC-PapersOnLine 2020;53(2):7338–43. http://dx.doi.org/10.1016/j.ifacol.2020.12.991, 21th IFAC World Congress.

[21] Boyd S, El Ghaoui L, Feron E, Balakrishnan V. Linear matrix inequalities in system and control theory. Society for Industrial and Applied Mathematics; 1994.
[22] Rotondo D, Nejjari F, Puig V. Design of parameter-scheduled state-feedback controllers using shifting specifications. J Franklin Inst B 2015;352(1):93–116.
[23] Chesi G, Garulli A, Tesi A, Vicino A. Robust stability of time-varying polytopic systems via parameter-dependent homogeneous Lyapunov functions. Automatica 2007;43(2):309–16.
[24] Geromel JC, Colaneri P. Robust stability of time varying polytopic systems. Systems Control Lett 2006;55(1):81–5.
[25] Oliveira RC, Bliman P-A, Peres PL. Robust LMIs with parameters in multi-simplex: Existence of solutions and applications. In: 2008 47th IEEE conference on decision and control. IEEE; 2008, p. 2226–31.
[26] Montagner VF, Oliveira RC, Peres PL, Bliman P-A. Stability analysis and gain-scheduled state feedback control for continuous-time systems with bounded parameter variations. Internat J Control 2009;82(6):1045–59.
[27] Dai D, Hu T, Teel AR, Zaccarian L. Piecewise-quadratic lyapunov functions for systems with deadzones or saturations. Systems Control Lett 2009;58(5):365–71.
[28] da Silva JMG, Tarbouriech S. Polyhedral regions of local stability for linear discrete-time systems with saturating controls. IEEE Trans Automat Control 1999;44(11):2081–5.
[29] Sala A, Arino C. Asymptotically necessary and sufficient conditions for stability and performance in fuzzy control: Applications of Pólya's theorem. Fuzzy Sets and Systems 2007;158(24):2671–86.
[30] Graham A. Kronecker products and matrix calculus with applications. Courier Dover Publications; 2018.
[31] Apkarian P, Gahinet P, Becker G. Self-scheduled $\mathcal{H}_\infty$ control of linear parameter-varying systems: a design example. Automatica 1995;31(9):1251–61.
[32] Nguyen A-T, Chevrel P, Claveau F. Gain-scheduled static output feedback control for saturated LPV systems with bounded parameter variations. Automatica 2018;89:420–4.
[33] Wu F, Yang XH, Packard A, Becker G. Induced L2-norm control for LPV systems with bounded parameter variation rates. Internat J Robust Nonlinear Control 1996;6(9–10):983–98.
[34] Löfberg J. YALMIP : A toolbox for modeling and optimization in MATLAB. In: 2004 IEEE international conference on robotics and automation (IEEE Cat. No.04CH37508). 2004, p. 284–9. http://dx.doi.org/10.1109/CACSD.2004.1393890.
[35] Sturm JF. Using SeDuMi 1.02, a MATLAB toolbox for optimization over symmetric cones. Optim Methods Softw 1999;11(1–4):625–53.
[36] Herceg M, Kvasnica M, Jones C, Morari M. Multi-parametric toolbox 3.0. In: Proc. of the european control conference. Zürich, Switzerland; 2013, p. 502–10, http://control.ee.ethz.ch/~mpt.
[37] Trapiello C, Puig V, Morcego B. Position-heading quadrotor control using LPV techniques. IET Control Theory Appl 2019;13(6):783–94.
[38] Rubí B, Ruiz A, Peréz R, Morcego B. Path-flyer: A benchmark of quadrotor path following algorithms. In: 2019 IEEE 15th international conference on control and automation (ICCA). 2019, p. 633–8. http://dx.doi.org/10.1109/ICCA.2019.8899563.